AIAA 81-4146

# Thermoplastic Behavior of a Thick-Walled Sphere

David Durban*
*Technion—Israel Institute of Technology, Haifa, Israel*

## Introduction

THE framework of small strain plasticity, in conjunction with the assumption of rigid plastic stress-strain relations, provides a useful model for assessing the plastic behavior of structures at sufficiently large strains. In this Note, we employ that model for analyzing the thermoplastic problem of a thick-walled sphere. An exact solution is obtained when the uniaxial stress-strain relation is described with a pure power law. The same problem has been studied in detail for an elastic-perfectly plastic material by Cowper[1] and Johnson and Mellor.[2]

Consider a thick-walled rigid-plastic sphere that is slowly heated by raising monotonously the temperature difference between the boundaries. Observing the spherical symmetry of the field and assuming (as will be verified later) continuous plastic loading along the deformation path, we can write the constitutive relations, e.g., Mendelson,[3] as

$$\epsilon_r = \alpha T - m\epsilon_p \tag{1}$$

$$\epsilon_\theta = \alpha T + \tfrac{1}{2} m\epsilon_p \tag{2}$$

where, with the usual notation for spherical coordinates, $\epsilon_r$ and $\epsilon_\theta$ are the strain components, $r$ is the radial coordinate, $\alpha$ the coefficient of thermal expansion, $T$ the temperature change, and $\epsilon_p$ the total plastic strain. The total plastic strain is related to the effective stress $\sigma_e$ through the pure power law

$$\sigma_e = K\epsilon_p^n \tag{3}$$

where $K$ and $n$ are material constants,

$$\sigma_e = -m(\sigma_r - \sigma_\theta) \qquad \text{with} \qquad m = -\operatorname{sgn}(\sigma_r - \sigma_\theta) \tag{4}$$

and $\sigma_r$, $\sigma_\theta$ are the stress components.

The strain displacement relations are

$$\epsilon_r = \mathrm{d}w/\mathrm{d}r \qquad \epsilon_\theta = w/r \tag{5}$$

where $w$ is the radial displacement. Combining Eqs. (5) gives the compatability equation

$$\frac{\mathrm{d}\epsilon_\theta}{\mathrm{d}r} - \frac{1}{r}(\epsilon_r - \epsilon_\theta) = 0 \tag{6}$$

Substituting Eqs. (1) and (2) in Eq. (6) results in the differential equation

$$\frac{\mathrm{d}\epsilon_p}{\mathrm{d}r} + \frac{3}{r}\epsilon_p = -2m\alpha\frac{\mathrm{d}T}{\mathrm{d}r} \tag{7}$$

Now, we assume that the radial temperature gradient is that of the steady-state temperature distribution, namely

$$\frac{\mathrm{d}T}{\mathrm{d}\rho} = -\Delta T\frac{k}{\rho^2} \tag{8}$$

Received Oct. 14, 1980; revision received Dec. 30, 1980. 

*Senior Lecturer, Dept. of Aeronautical Engineering.

with

$$\rho = r/\sqrt{ab} \qquad k = \sqrt{\beta}/(\beta - 1) \qquad \beta = b/a \tag{9}$$

where $a$ and $b$ are the inner and outer radii, respectively, and $\Delta T$ is the (positive) temperature difference between these radii.

Substituting Eq. (8) in Eq. (7) and solving for $\epsilon_p$ with the initial condition $\epsilon_p = 0$ at $\rho = \rho_0$, we find that the shell is divided into two parts, with the interface $\rho = \rho_0$, according to the sign of $(\sigma_r - \sigma_\theta)$:

$$\epsilon_p = \theta k\left(\frac{\rho_0^2}{\rho^3} - \frac{1}{\rho}\right) \qquad \text{for } \frac{1}{\sqrt{\beta}} \le \rho \le \rho_0,\ m = -1 \tag{10a}$$

$$\epsilon_p = \theta k\left(\frac{1}{\rho} - \frac{\rho_0^2}{\rho^3}\right) \qquad \text{for } \rho_0 \le \rho \le \sqrt{\beta},\ m = 1 \tag{10b}$$

where

$$\theta = \alpha\Delta T \tag{11}$$

The corresponding expressions for the effective stress follow now from Eqs. (3) and (4) as

$$\sigma_e = \sigma_r - \sigma_\theta = K\theta^n k^n\left(\frac{\rho_0^2}{\rho^3} - \frac{1}{\rho}\right)^n \text{ for } 1/\sqrt{\beta} \le \rho \le \rho_0 \tag{12a}$$

$$\sigma_e = \sigma_\theta - \sigma_r = K\theta^n k^n\left(\frac{1}{\rho} - \frac{\rho_0^2}{\rho^3}\right)^n \text{ for } \rho_0 \le \rho \le \sqrt{\beta} \tag{12b}$$

Note that at the interface, the state of stress is purely hydrostatic. The location of the interface is as yet unknown, but, as we proceed to show below, the value of $\rho_0$ is uniquely determined by the thickness ratio $\beta$ and by the hardening parameter $n$.

The equation of equilibrium, when combined with Eq. (4), is

$$\frac{\mathrm{d}\sigma_r}{\mathrm{d}\rho} = -\frac{2}{\rho}(\sigma_r - \sigma_\theta) = 2m\frac{\sigma_e}{\rho} \tag{13}$$

Substituting $\sigma_e$ from Eq. (12) in Eq. (13) and integrating over $\rho$ with the initial conditons

$$\sigma_r = 0 \text{ at } \rho = 1/\sqrt{\beta} \text{ and at } \rho = \sqrt{\beta} \tag{14}$$

gives

$$\sigma_r = -2K\theta^n k^n \int_{1/\sqrt{\beta}}^{\rho}\left(\frac{\rho_0^2}{\rho^3} - \frac{1}{\rho}\right)^n\frac{\mathrm{d}\rho}{\rho} \text{ for } 1/\sqrt{\beta} \le \rho \le \rho_0 \tag{15a}$$

$$\sigma_r = -2K\theta^n k^n \int_{\rho}^{\sqrt{\beta}}\left(\frac{1}{\rho} - \frac{\rho_0^2}{\rho^3}\right)^n\frac{\mathrm{d}\rho}{\rho} \text{ for } \rho_0 \le \rho \le \sqrt{\beta} \tag{15b}$$

The requirement for continuity of radial stress at the interface now leads to the transcendental equation

$$\int_{1/\sqrt{\beta}}^{\rho_0}\left(\frac{\rho_0^2}{\rho^3} - \frac{1}{\rho}\right)^n\frac{\mathrm{d}\rho}{\rho} = \int_{\rho_0}^{\sqrt{\beta}}\left(\frac{1}{\rho} - \frac{\rho_0^2}{\rho^3}\right)^n\frac{\mathrm{d}\rho}{\rho} \tag{16}$$

from which $\rho_0$ is determined. The fact that the location of the interface is independent of temperature verifies the assumption of continuous plastic loading.

For a given value of $\beta$, it is possible to solve Eq. (16) numerically, using a standard Newton-Raphson method, and obtain the corresponding value of $\rho_0$. The dependence of $\rho_0$

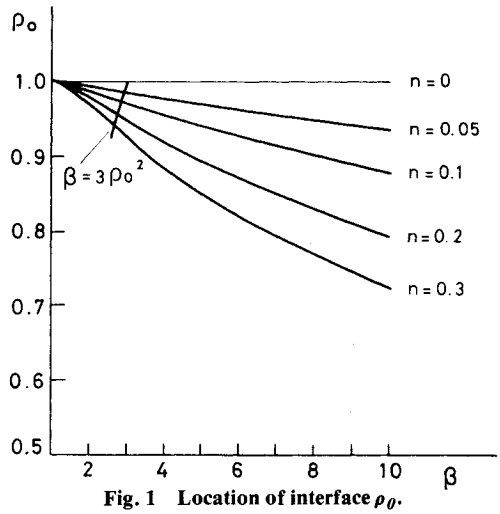


**Fig. 1 Location of interface $\rho_0$.**

on the radii ratio $\beta$ is displayed in Fig. 1 over the practical range of the hardening parameter $n$. Typical values of $n$ are $n=0.25$ (soft aluminum), $n=0.2$ (killed steel), $n=0.092$ (aluminum 7075 T6), $n=0.06$ (steel 5 CrMoV), and $n=0.029$ (steel X-200). We can conclude from Fig. 1 that the interface location moves inward toward the inner boundary as $\beta$ and $n$ increase. Note that with $n=0$, the solution of Eq. (16), namely $\rho_0=1$, agrees with Cowper's[1] result for a rigid-perfectly plastic material.

The radial stress can now be found directly from Eqs. (15). The circumferential stress distribution is then obtained by combining Eqs. (15) and (12):

$$\sigma_\theta = -K\theta^n k^n\left[\left(\frac{\rho_0^2}{\rho^3}-\frac{1}{\rho}\right)^n + 2\int_{1/\sqrt{\beta}}^{\rho}\left(\frac{\rho_0^2}{\rho^3}-\frac{1}{\rho}\right)^n\frac{d\rho}{\rho}\right]$$

$$\text{for } \frac{1}{\sqrt{\beta}} \le \rho \le \rho_0 \tag{17a}$$

$$\sigma_\theta = K\theta^n k^n\left[\left(\frac{1}{\rho}-\frac{\rho_0^2}{\rho^3}\right)^n - 2\int_{\rho}^{\sqrt{\beta}}\left(\frac{1}{\rho}-\frac{\rho_0^2}{\rho^3}\right)^n\frac{d\rho}{\rho}\right]$$

$$\text{for } \rho_0 \le \rho \le \sqrt{\beta} \tag{17b}$$

The stresses increase proportionally with $\theta^n$, but their radial profile is independent of the temperature. In discussing the stress distributions, it is convenient to transform to the new radial coordinate

$$R = \frac{\sqrt{\beta}\rho - 1}{\beta - 1} - \frac{1}{2} \tag{18}$$

so that the radial range is now $[-\frac{1}{2},\frac{1}{2}]$ regardless of the thickness ratio. Typical stress fields are shown in Figs. 2 for two representative shells. An immediate conclusion that follows from these figures is that for the same material and temperature difference, $\theta$, the stresses reach higher values in the thicker shell. The location of the interface in Figs. 2 is indicated by the intersection of the curves for $\sigma_r$ and $\sigma_\theta$. Note that, in agreement with Eqs. (15), $|\sigma_r|_{\max}$ occurs exactly at the interface. The largest absolute stress is attained by the circumferential component $|\sigma_\theta|$ between the inner surface ($\rho = 1/\sqrt{\beta}$) and the interface ($\rho=\rho_0$). The location of that extremum (minimum) is easily obtained from Eq. (17a) as

$$\rho\sqrt{(2-3n)/(2-n)}\,\rho_0 \tag{19}$$

Equation (19) is valid for shells where $\sqrt{\beta}\rho_0 > \sqrt{(2-n)/(2-3n)}$. In thinner shells, where $\sqrt{\beta}\rho_0 \le \sqrt{(2-n)/(2-3n)}$, the location of $|\sigma_\theta|_{\max}$ is at the inner surface.

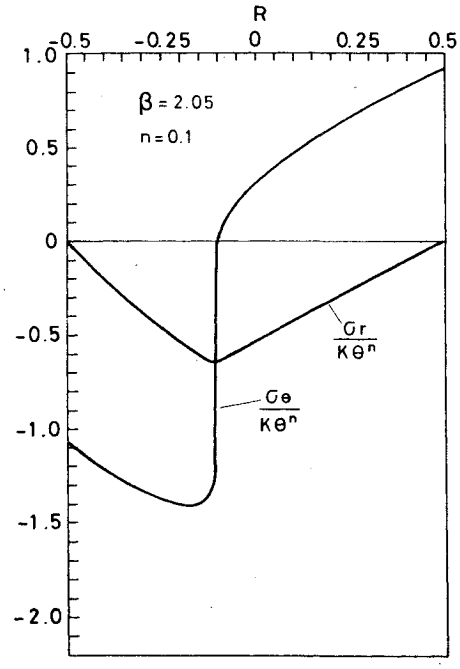


**Fig. 2a Stress distributions, $\beta=2.05$, $n=0.1$; curves intersect at interface $\rho_0$.**

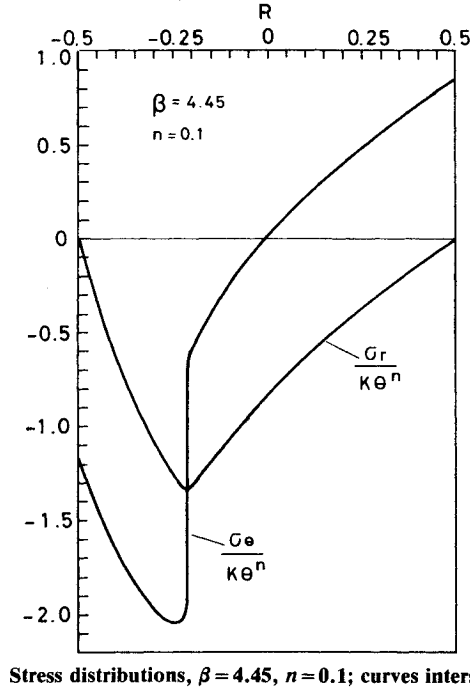


**Fig. 2b Stress distributions, $\beta=4.45$, $n=0.1$; curves intersect at the interface $\rho_0$.**

It can be verified from Eqs. (12), that the highest effective stress is always at the inner surface. However, for sufficiently thick shells, the effective stress has a second maximum within the shell at $\rho=\sqrt{3}\rho_0$, as can be seen from Eq. (12b). Such a maximum will occur only in shells where $\beta > 3\rho_0^2$, i.e., on the right side of the curve $\beta=3\rho_0^2$ shown in Fig. 1. That inequality can be compared with the result by Cowper[1] that a second plastic zone starts to develop within an elastic-perfectly plastic shell provided that $\beta > 2.791$.

The radial displacement can be expressed in a single formula for the whole shell by combining Eqs. (2) and (5) with Eqs. (10), resulting in

$$\frac{w}{\sqrt{ab}} = \alpha T\rho + \frac{1}{2}\theta k\left(1-\frac{\rho_0^2}{\rho^2}\right) \tag{20}$$

The present analysis reveals the essential plastic behavior of the sphere at sufficiently high temperatures. For an elastoplastic material, however, we can expect a thin elastic zone to exist near $\rho_0$. Assuming that this zone is bounded by $\rho=\rho_0(1\pm\frac{1}{2}\delta)$ where $\delta\ll 1$, and that $\epsilon_p$ at the boundaries of that elastic zone is equal to the yield strain $\epsilon_y$, we find from Eqs. (10) by a simple expansion that $\delta\approx\rho_0\epsilon_y/\theta k$. By comparison, the result given by Cowper[1] for an elastic-perfectly plastic material reads, with the present notation, $\delta\approx 2(1-\nu)\epsilon_y/\theta k$. Both expressions for $\delta$ coincide with $n=0$ and $\nu=\frac{1}{2}$, respectively.

Finally, we mention that the present analysis is not restricted to the steady-state temperature distribution and can easily be repeated with other radial temperature gradients.

## References

[1] Cowper, G. R. "The Elastoplastic Thick-Walled Sphere Subjected to a Radial Temperature Gradient," *Journal of Applied Mechanics*, Vol. 27, Sept. 1960, pp. 496-500.

[2] Johnson, W. and Mellor, P. B., "Elastic-Plastic Behaviour of Thick-Walled Spheres of Non-Work-Hardening Material Subject to a Steady State Radial Temperature Gradient," *International Journal of Mechanical Sciences*, Vol. 4, March-April 1962, pp. 147-158.

[3] Mendelson, A., *Plasticity: Theory and Application*, The MacMillan Company, New York, 1968, pp. 135-137.

AIAA 81-4147

# Effect of Stiffener Eccentricity in Axially Compressed Waffle Cylinders

R. Karmakar*
*Indian Institute of Technology, Kharagpur, India*

## Nomenclature

| | |
|---|---|
| $A_a, A_c, A_s$ | = axial, circumferential, and spiral stiffener area |
| $a$ | = stiffener grid size |
| $B$ | = extensional rigidity of plate, $Eh/(1-\nu^2)$ |
| $C_i$ | = stiffness parameters |
| $D$ | = bending rigidity of plate, $Eh^3/12(1-\nu^2)$ |
| $d$ | = stiffener depth |
| $E$ | = Young's modulus |
| $h$ | = skin thickness |
| $I_a, I_c, I_s$ | = moment of inertia of axial, circumferential, and spiral stiffener area about shell reference line |
| $L$ | = cylinder length |
| $N_{xcr}$ | = buckling load |
| $\bar{N}$ | = nondimensional buckling load, $N_{xcr}/ER$ |
| $R$ | = cylinder radius |
| $t_a, t_c, t_s$ | = axial, circumferential, and spiral stiffener thickness |
| $t_{eq}$ | = equivalent shell thickness |
| $\bar{t}$ | = nondimensional equivalent thickness, $t_{eq}/R$ |
| $\alpha$ | = helix angle of spiral stiffener |
| $\epsilon_1, \epsilon_2, \gamma$ | = reference surface strains |
| $\chi_x, \chi_y, \chi_{xy}$ | = changes of curvature |

## Introduction

THE eccentricity of stiffeners has a large effect on the critical load in cylindrical shells and outside stiffening has been found to be stronger than inside stiffening.[1-4] Inversion of the stiffener eccentricity effect has been observed in cylinders under hydrostatic pressure loading.[5,6] Singer et al.[6] explained that stiffener eccentricity has two opposing effects. The primary effect is that the actual bending stiffness for outside stiffening is larger than that for inside stiffening. The secondary effect is that the actual extensional stiffness in the circumferential direction for inside stiffening is more than that for outside stiffening. This secondary effect arises out of Poisson's effect.

If the stiffener depth in a waffle cylinder is increased, the eccentricity and second moment of area of the stiffener increase. The consequent increase in actual bending stiffness causes the buckling load to increase monotonically with increase in stiffener depth.[1] The primary effect of stiffener eccentricity increases the buckling load for outside stiffening while the secondary effect decreases the same. A possible variation of the change in buckling load due to the secondary effect is shown in Fig. 1.[1] Thus, for a predominant primary effect, outside stiffening is stronger and a predominant secondary effect may cause an inversion of the stiffener eccentricity effect. This inversion is represented graphically in Fig. 2.

In this Note waffle cylinders with spiral-cum-orthogonal stiffener configuration (Fig. 3) have been analyzed for buckling under uniform axial compression. It is observed that inversion of the stiffener eccentricity effect may also occur under axial compression for this type of stiffener configuration and that the inversion is influenced by Poisson's ratio of the cylinder material.

## Analysis

In an eccentrically stiffened shell-wall construction there is a coupling between extensional forces and curvature change and between bending moments and extensional strains. To account for this coupling the resultant forces and moments on a shell element may be generalized to the form

$$\begin{aligned} N_x &= C_1\epsilon_1 + C_2\epsilon_2 + C_3\chi_x + C_4\chi_y \\ N_y &= C_5\epsilon_1 + C_6\epsilon_2 + C_7\chi_x + C_8\chi_y \\ N_{xy} &= N_{yx} = C_9\gamma + C_{10}\chi_{xy} \\ M_x &= C_{11}\epsilon_1 + C_{12}\epsilon_2 + C_{13}\chi_x + C_{14}\chi_y \\ M_y &= C_{15}\epsilon_1 + C_{16}\epsilon_2 + C_{17}\chi_x + C_{18}\chi_y \\ M_{xy} &= -M_{yx} = C_{19}\gamma + C_{20}\chi_{xy} \end{aligned} \tag{1}$$

Using the method outlined in Ref. 1, the stiffness parameters are obtained as

$$C_1 = B + KA_{sa}T_1/t_{sa} \qquad C_2 = B\nu + KA_{sa}/t_{sa}$$

$$C_3 = -KA_{sa}T_1 e/t_{sa} \qquad C_4 = -KA_{sa}e/t_{sa}$$

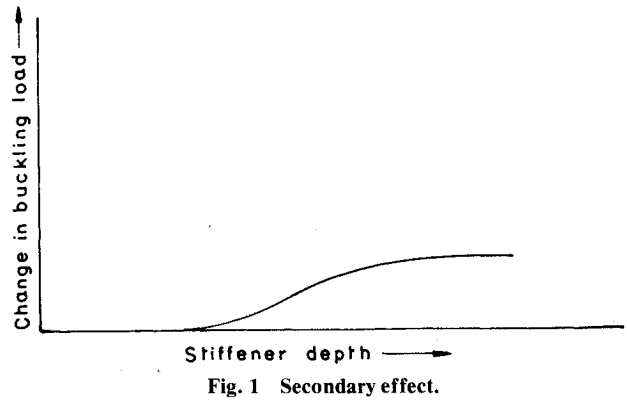


**Fig. 1 Secondary effect.**

Received Jan. 3, 1980; revision received Dec. 8, 1980. 

*Lecturer, Department of Aeronautical Engineering.